Chapter 15
Variable Atwood Number Rayleigh-Taylor InstabilitiesInduced by Volumetric Energy Deposition

Clara S. Bender, Anna C. Cardall, Fabian A. Rodriguez, Joseph A. Kerwin, Ricardo Mejia, and Adam J. Wachtor

Abstract Instabilities similar to the Rayleigh-Taylor instability (RTI) are inherent to internal confinement fusion (ICF) during the compression of target fuel capsules and ultimately lead to a reduction of fuel efficiency. While computational models for RTI in the context of ICF exist, lab-scale experimental work is needed to validate the assumptions and results of these models. Much experimental work investigating RTI has been performed, but few studies involve the condition of volumetric heating or the resultant temporal variation in fluid density that is present in ICF. This work investigated RTI induced by microwave volumetric energy deposition (VED), which caused buoyancy-driven mixing due to density stratification inversion. Experimentation involved a vessel with an initially stable system of two stratified immiscible fluids with different densities. As the two-fluid system was heated and heat transferred from the top fluid to the bottom fluid, the initially denser bottom fluid experienced preferential thermal expansion at the fluid interface, inducing buoyancy-driven mixing. The temperature at various points in the fluids was recorded using fiber optic temperature probes, and the temperature data were then used to calculate density. It was found that density inversion did not occur at the temperature probe locations, but the data support the hypothesis that density inversion occurred close to the fluid interface. Since the refractive indexes of the fluids are different, the phenomenon was visualized with shadowgraph videography. Once the mixing process was recorded, images were processed with edge detection and motion tracking techniques. Image processing was used to unveil the presence of morphological features of the flow such as spikes and bubbles and to quantify the evolution of the wave properties. The results were compared to traditional RT equations, and it was found that initial wave amplitude growth agreed with traditional RT literature, while the later stage was inconsistent with traditional RT literature.

Keywords Rayleigh-Taylor instability · Unstable stratification · Volumetric energy deposition · Microwaves

Introduction

Hydrodynamic instabilities have long been studied because of their relevance in several physical processes, including challenges such as geological storage of CO_2 [1], multi-phase chemical reactions [2], droplet breakup [3, 4], and inertial confinement fusion (ICF). This work primarily addresses the challenges found in ICF, where development has been hindered by a lack of understanding of the hydrodynamic instabilities inherent to the process [5]. In ICF, a spherical fuel capsule containing a deuterium-tritium (DT) core is bombarded with x-rays, which initiates a shock wave travelling radially inward. The shock wave heats and compresses the DT core to initiate a fusion reaction [6]. During this process, the fuel capsule shell is vaporized into plasma, and the surface irregularity of the shell combined with the shock wave causes mixing of the plasma and the DT fuel, causing some of the fuel to escape the highly pressurized and heated center before it can fuse. The

Clara S. Bender · Anna C. Cardall · Fabian A. Rodriguez · Adam J. Wachto
Engineering Institute Los Alamos National Laboratory
e-mail: csbender@lanl.gov; cardalla@lanl.gov; fabian.rodriguez@lanl.gov; ajw@lanl.gov

Joseph A. Kerwin
Test Engineering Group | Los Alamos National Laboratory
e-mail: jkerwin@lanl.gov

Ricardo Mejia
Department of Mechanical Engineering Michigan State University
e-mail: rimejal@msu.edu

Matthew Allen et al. (eds.), *Special Topics in Structural Dynamics & Experimental Techniques, Vol. 5*, Conference Proceedings of the Society for Experimental Mechanics Series, https://doi.org/10.13052/97887-438-0150-4_15

hydrodynamic instability at the interface between the plasma and capsule shell after the shock demonstrates similar fluid dynamic behavior to Rayleigh-Taylor instability (RTI).

RTI has been studied extensively to further understand the ICF process. Traditionally, RTI experiments and simulations involve an initially stratified system of two fluids of different densities in a gravitational or acceleration field. A measure of the buoyancy of the bottom fluid in the top fluid is given by the dimensionless Atwood number, At:

$$At=\frac{\rho_1-\rho_2}{\rho_1+\rho_2}, \tag{1}$$

where ρ_1 and ρ_2 are the densities of the top and bottom fluids in the system, respectively. In the presence of an acceleration field such as gravity, the system is considered unstable when At is positive (i.e., when the top fluid is denser than the bottom fluid, and $\rho_1 > \rho_2$). Surface tension maintains the initial state until there is a perturbation (disturbance) at the interface. Then, gravity acts to propagate the disturbance towards the stable state where the denser fluid rests at the bottom of the system. For a perturbation with amplitude η and wavelength λ in a simple system of two immiscible and incompressible fluids, the initial growth rate of small amplitude perturbation, i.e. ($\eta_o \ll \lambda$), is given by Eq. (2), where g is a constant acceleration (often gravity) [7].

$$\eta\left(t\right) = \eta_o \bullet \exp\left[\left(\frac{2 \bullet \pi \bullet \mathrm{At} \bullet \mathrm{g}}{\lambda}\right)^{1/2} \bullet \mathrm{t}\right] \tag{2}$$

As mixing progresses, η and λ become similar, η is thought to grow at a constant rate [7, 8]. Further in time, the perturbations become broadband and chaotic in nature, a mixing region of height h develops. At this stage, $h \gg \lambda_m$, where λ_m is the maximum wavelength of the initial perturbations [7, 8]. In idealized conditions (where the viscous and diffusion length scales are much less than h), the growth of h is given by

$$h\left(t\right) \approx \alpha \bullet At \bullet g \bullet t^2. \tag{3}$$

In this traditional understanding of RTI, the density of each fluid is constant (and thus At is constant). However, in ICF, constant volumetric energy deposition (VED) imparted by fusion products (neutrons and alpha particles) and the incoming x-rays cause thermal expansion and subsequent density variation of pellet materials. This creates a situation in which At varies with time (Eq. (4)).

$$At\left(t\right) = \frac{\rho_1\left(t\right) - \rho_2\left(t\right)}{\rho_1\left(t\right) + \rho_2\left(t\right)} \tag{4}$$

Some work has been done to demonstrate variable At, VED-driven RTI at the lab scale. Joshi et al. [9] investigated VED-driven RTI using dielectric fluids in a nonuniform electric field, where one fluid is preferentially heated due to its permanent or induced dipole. Wachtor et al. [10] demonstrated this result experimentally with microwave-driven RT mixing of two miscible fluids. In another experiment, it was demonstrated that the mixing layer growth rate in VED-driven RTI is increased over the classical RT t^2 scaling of Eq. (3) [11]. Recently, Root et al. [12] demonstrated RT mixing of two immiscible fluids through microwave heating, leveraging the different refractive indexes to obtain shadowgraph videography of the growth of perturbations. There has yet to be an experiment that collects and analyzes thermal and video data resulting from RTI between two immiscible fluids through microwave heating to perform a quantitative comparison to classical RTI literature.

The focus of this work is to further inform modeling RTI in ICF with an improved experiment involving microwave heating of two immiscible fluids. The experimental setup was designed to reduce the 3D effects of the mixing and isolate the early stages of RTI described by Eq. (2) and Eq. (3). Temperature data were collected at a vertical cross-section of the fluids and utilized to calculate the fluid density gradient during mixing. Processing and analysis of video capturing the mixing process allowed for the quantification of perturbation amplitude growth, which was compared to the traditional, constant At RT models.

Methods

Fluid Selection

Fluid selection was based on work performed by *Root et al. [12]*, who demonstrated VED-driven RTI using 7 cSt polydimethylsiloxane (PDMS) and soybean oil. The pair was chosen based on their immiscibility, sufficient microwave penetration depths for the fluid vessel, and capability of density inversion through heating. The fluids' immiscibility improves the visibility of the RT*I* behavior and isolates macroscopic behavior with the tradeoff of introducing interfacial tension effects.

The 7 cSt PDMS is the denser of the pair at an ambient temperature of ∼25°C, but for any shared temperature above 43°C, soybean oil is denser (Figure 1). Both fluids are also non-hazardous. Soybean oil is primarily composed of triacylglycerols, a type of lipid. PDMS is a linear-chain polymer with chemical formula $(SiO(CH_3)_2)_x$, whose length dictates its viscosity *[13]*. The combination of 7 cSt PDMS and soybean oil was found to support RTI development as demonstrated by *[12]* and was used in the experiments reported below. Each fluid's density as a function of temperature in Figure 1 was used to estimate the fluid density over time during mixing from collected temperature measurements.

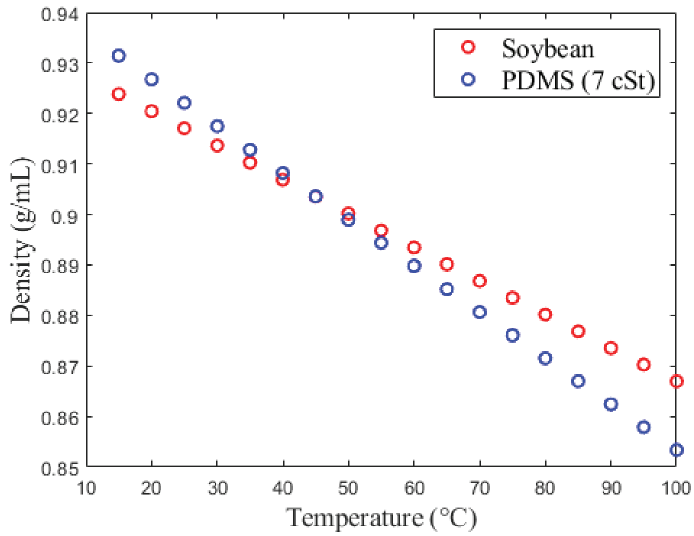

Fig. 1 Density as a function of temperature for soybean oil (Thermo Scientific Chemicals, A12728.0E) and 7cSt PDMS (Gelest, DMS-T07-KG) as measured using a densitometer (Anton Paar; Model: Modulyzer Polymers).

Experimental Setup

A custom, rectangular quartz vessel was used to contain the fluids. Quartz is optically transparent, thermally resistant in comparison to other glasses, and has low dielectric loss, making it an ideal vessel material for the microwave heating experiments and video imaging. The vessel had external dimensions of 150.01 mm (length – L) x 21.35 mm (width – W) x 152.40 mm (height – H). All vessel walls were 3.175 mm thick, giving an internal vessel width of 15 mm. The internal width of 15 mm was chosen, because a video image from [12] shows the base of a spike to be about 15 mm. The goal was to produce a system as 2-dimensional as possible while minimizing wall effects. A Teflon stand was constructed to stabilize the thin fluid vessel. Like quartz, Teflon was also chosen for its low microwave absorption. Fiber optic temperature probes (Omega Engineering Inc., FOS-LU-2) connected to a data logger (Omega Engineering Inc., FOM-H201) were utilized to collect temperature data with an accuracy of ± 0.8°C.

A large format microwave (Microwave Research and Applications, Inc, Model BP-210) was used to supply VED to the fluids. The microwave has an operating frequency of 2.45 GHz and maximum power output of 2,100 Watts, and its cavity has dimensions of 53.5 cm (W) x 33.0 cm (L) x 25.1 cm (H). Three 3.8 cm diameter access ports were added to the microwave — one on each side and another on the door — for the purpose of imaging. The access port on the left side was used to provide LED backlighting to the vessel (Nila, Model NZL1D-D). A piece of parchment paper taped against left port and a 0.635-cm thick Teflon plate placed next to the vessel diffused the backlighting to provide more even backlighting to the two-fluid system. A CMOS camera (Point Grey, Model GS3-U3-23S6M-C) and a focusing lens (Fujinon, Model HF35SA-1) placed through the access port on the right side of the microwave door were used to obtain grayscale, 10 frames per second (fps) videos of the mixing process (Figure 2).

Single-Fluid Calibration Procedure

To develop an understanding of how each fluid would change temperature over time for a given microwave power level and vessel, single-fluid calibration experiments were conducted. Only measurements conducted at a microwave power level of 840 W (40% of the microwave's maximum power) are reported in this work. The fluids' microwave penetration depths

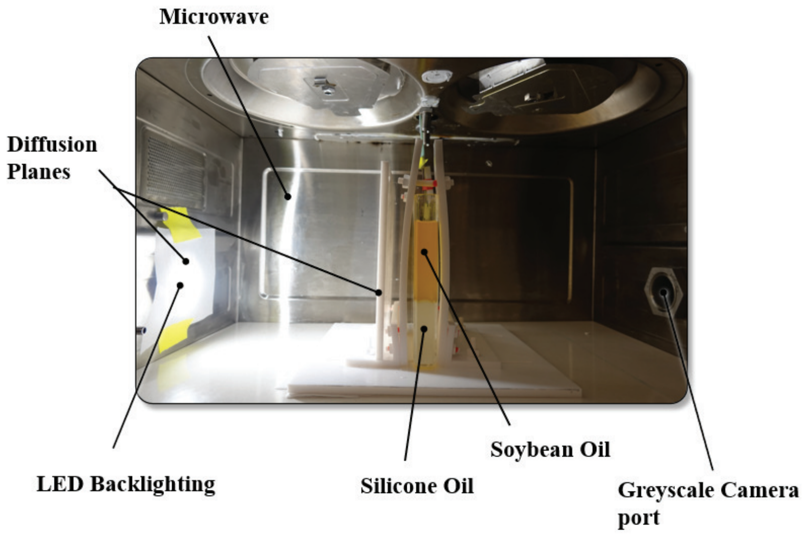

Fig. 2 Experimental setup of two-fluid system in the microwave cavity.

were much larger than the dimensions of the vessel and the total fluid volume for the single-fluid experiments was chosen to be equal to that of the mixing experiments. As such, the single-fluid temperature data were intended inform the fluid temperatures during the mixing experiments. 270 mL of each oil was heated from room temperature (between 19 °C and 23 °C) in the quartz vessel for 3000 seconds. Six fiber optic temperature probes were fed through 4mm diameter holes spaced 16 mm apart in a 0.635-cm thick Teflon plate resting on top of the vessel (Figure 3). The tips of the probes reached approximately halfway down into the fluid. The temperature measurement from each probe was recorded at a frequency of 1 Hz. Three trials were performed for each fluid.

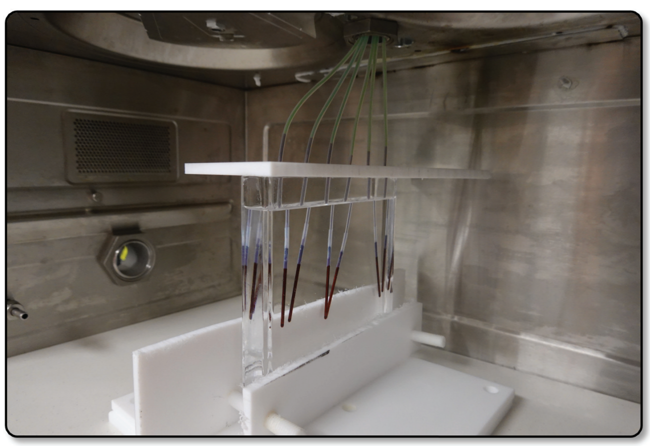

Fig. 3 Single-fluid calibration setup. Six fiber optic temperature probes were distributed along the length of the fluid vessel.

Rayleigh-Taylor Mixing Experiment Procedure

For mixing experiments, an equal volume (135 mL) of room temperature (∼21 °C) soybean oil and PDMS were loaded into the vessel. Soybean oil was poured in the vessel first, then the initially denser PDMS was loaded into the bottom of the vessel using a syringe and tube. The vessel was secured in the Teflon stand, and the microwave was powered at ∼840 W for 3000 seconds. Six temperature probes were placed outside the field of view of the camera at incremental heights in the fluids, with three in the bottom fluid and three in the top fluid (Figure 4). The temperature data was then used to calculate the fluid densities over time at each measurement height using relationships between density and temperature data found for each fluid.

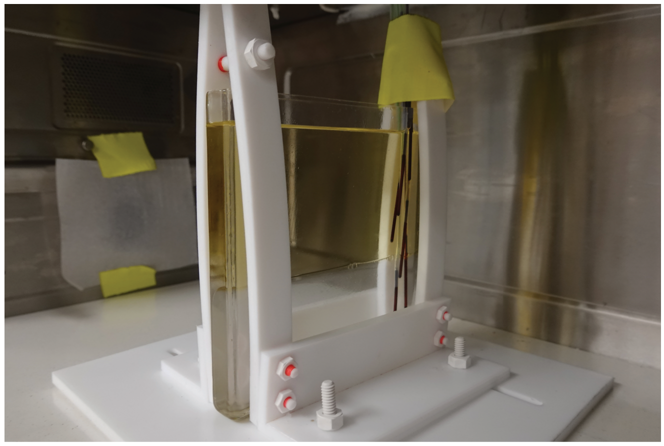

Fig. 4 VED RTI mixing experimental setup before the Teflon diffusing plane was inserted into the microwave cavity.

Image Processing

An image processing workflow was applied to the videos of the mixing process to characterize the evolution of the fluid interface (Figure 5). Preprocessing steps included cropping the video frames to a region of interest, background correction to account for uneven backlighting (Figure 5b-c), and smoothing to reduce noise and enhance the fluid interface (Figure 5f). Background correction was performed by using an iterative Gaussian smoothing filter on each raw image (Figure 5a) to

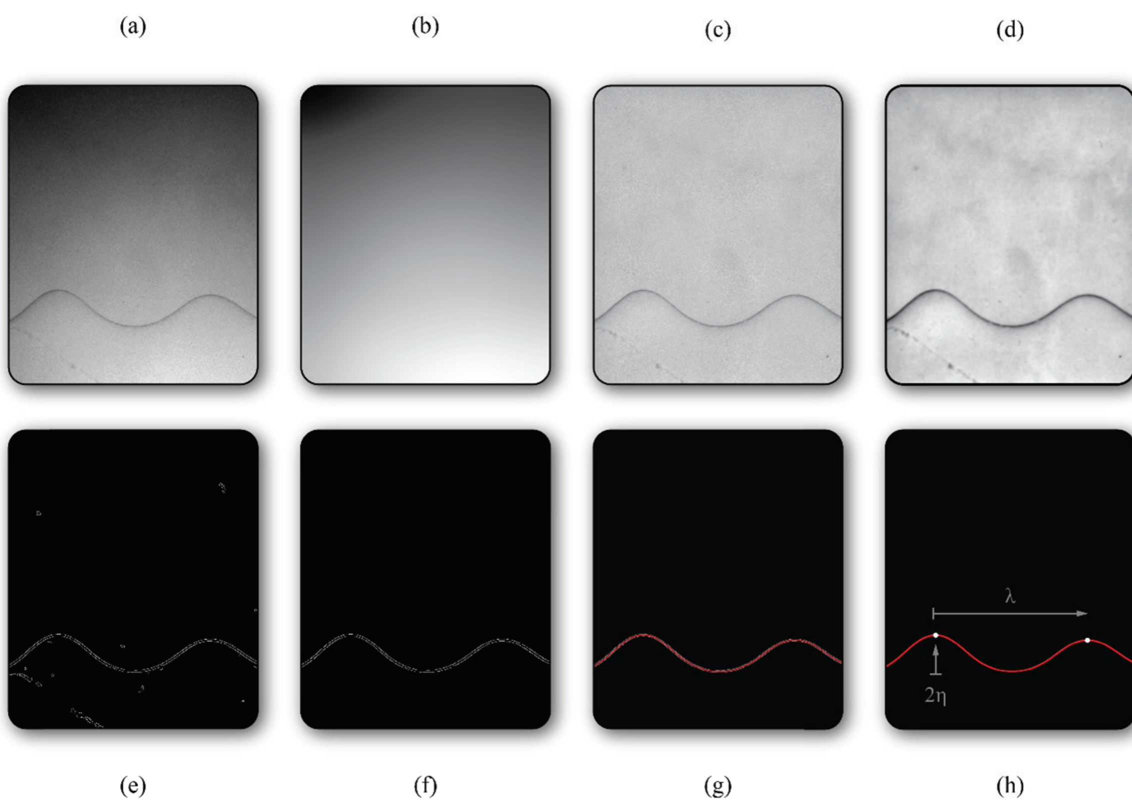

Fig. 5 The image processing workflow used to extract the amplitude (η) and wavelength (λ) of the the wavelike fluid interface. (a) Raw video frame, (b) estimation of the uneven backlighting, (c) frame corrected for uneven backlighting, (d) smoothed image to enhance the fluid interface and remove noise, (e) result of Canny edge detection, (f) cleaned edge detection image, (g) interface estimate using a piecewise polynomial (spline), and (g) estimate η and λ from automated image analysis workflow.

capture the background produced by uneven backlighting (Figure 5b). The raw image was then corrected using the estimated background to produce an image where contrast is concentrated at the fluid interface (Figure 5c). Smoothing was performed via guided filtering, technique used to reduce noise while preserving the sharpness of edges. Canny edge detection was then used to locate the fluid interface (Figure 5e). Noise in the resulting binary image was reduced using a tuned cleanup step in which long, continuous edges were preserved, and short edges were removed (Figure 5f).

The pixels identified as the fluid interface were used to obtain η and λ. The locations of edge pixels were used to fit a piecewise polynomial (or spline, Figure 5g). Smoothing of the spline was adjusted to capture the curvature of the wave while avoiding overfitting. The distance between the minimum and maximum of the spline was considered 2η, and the distance between the maxima of the wavelike interface was considered λ (Figure 5h). The maxima were found by computing the first and second derivatives of the spline and selecting those points whose first derivative was approximately zero and second derivative was negative. In some cases, the λ was instead calculated using the minima, which was done using the same procedure but with a positive second derivative condition.

The image processing workflow was automated and applied to each frame in the videos capturing the mixing process. The evolution of η and λ in time was tracked. Curves for η versus time were fit for two periods during the mixing process: when $\eta \ll \lambda$ and when $\eta \approx \lambda$ (the threshold defined at $0.1\ \lambda$).

Results

Single-Fluid Calibration

Six temperature probes captured the temperature of each isolated fluid while heated in the microwave. The temperature evolution followed the shape of a decaying exponential, with the soybean oil having a much higher end temperature and time constant than 7cSt PDMS (Figure 6). For each trial, it was found that the variation in temperature between various probes increased over time and reached a maximum of less than 10% of the increased temperature difference ($\sim$10 °C for soybean oil, $\sim$3 °C for the 7cSt PDMS). When the single-fluid temperature data was combined with fluid density-temperature to estimate the *At* variation, it was found that the fluid system would never an unstable configuration under the assumption that the mixing fluid temperatures would be equivalent to the single-fluid calibration temperatures (Figure 7).

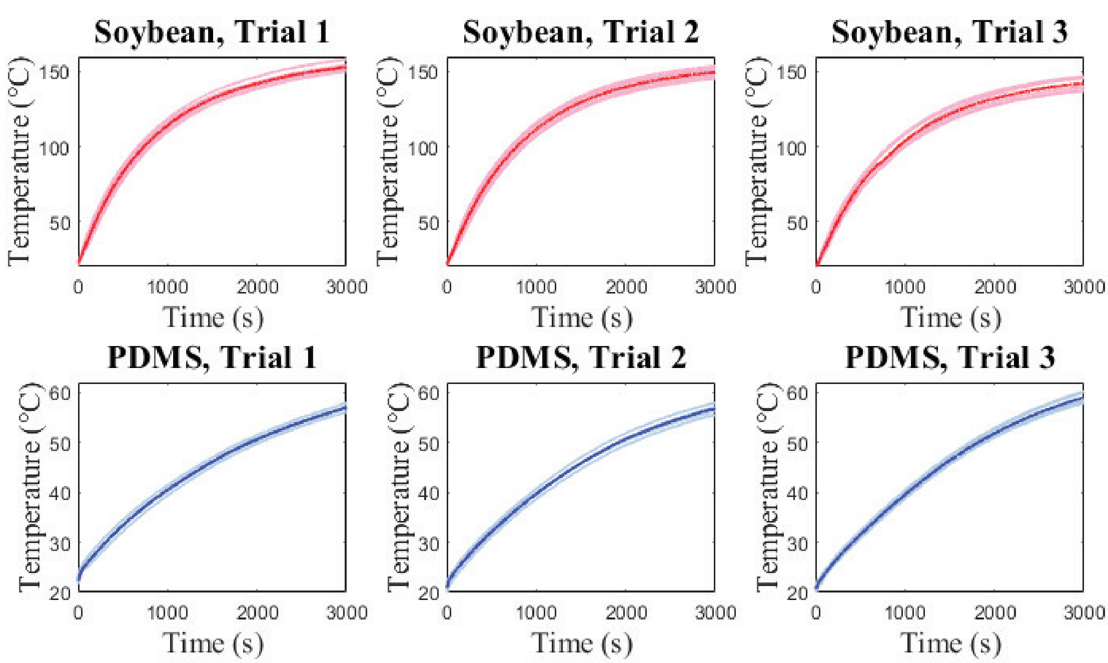

Fig. 6 Single-fluid calibration temperature curves for soybean oil (red) and PDMS (blue) heated at 840 W. Lighter lines indicate individual temperature probes and bold lines represent the average temperature over all the probes for that trial.

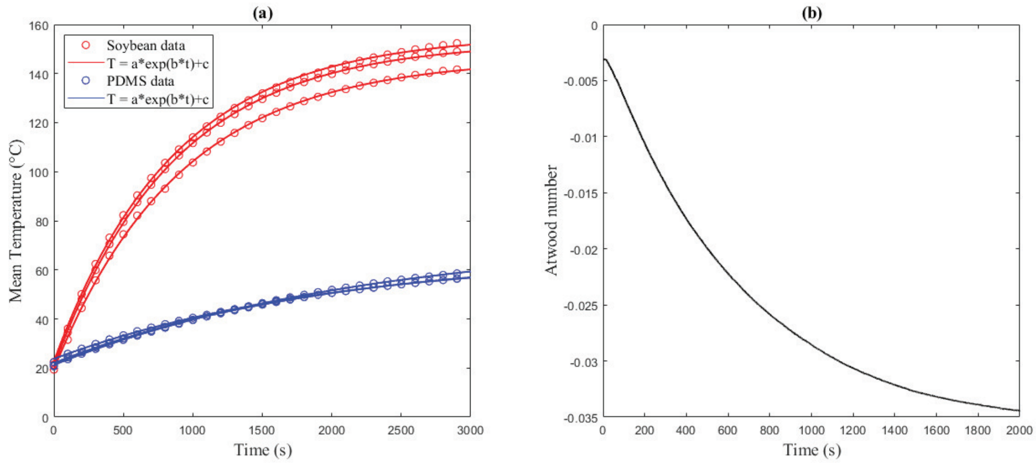

Fig. 7 (a) Average temperatures for all single-fluid trials with decaying exponential fits. (b) Estimated Atwood number determined using single-fluid temperature measurements and density-temperature relationship measured in Figure 1.

VED Mixing Experiment

Temperature probes were aligned vertically in the two-fluid system outside the field-of-view of the imaging system to capture the temperature of each fluid at the top, middle, and bottom of each respective fluid. As in the single-fluid experiments, the soybean oil exhibited higher overall temperatures than the PDMS. The middle region of each fluid reached a maximum temperature difference of about 50 °C after 900 seconds at the neighboring probe locations. During this time, the soybean oil exhibited a temperature difference of ∼20 °C from the top of the fluid to near the fluid interface, while the PDMS exhibited an increase in temperature ∼12 °C between the bottom and the near fluid interface (Figure 8a).

The shadowgraph video of the mixing process captured the fluid interface well. An initial single wavelength perturbation began at about 600 seconds, which grew in amplitude until the PDMS spikes experienced necking and bubbles separated from the vertical fluid jets. As fluid heating continued, the spikes cyclically grew, necked, and broke off into bubbles (Figure 9).

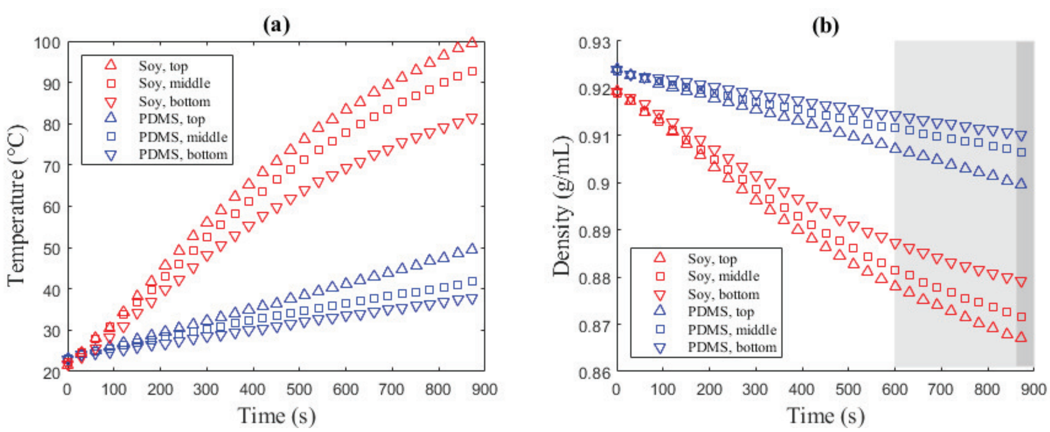

Fig. 8 Temperature data (a) and estimated density (b) versus time for RT mixing experiment. The light grey area in the density graph indicates the time region in which video footage showed growing perturbations, while the dark grey area indicates the time region of bubble formation.

Image processing and analysis of the mixing experiment reveal growth in η and a decrease in λ, as shown in Figure 10. Analysis was limited to a specific timeframe of interest, beginning around 600 s (when the initial perturbation at the interface was detected) and ending at 840 s (when bubble separation began to occur). Some noise is present near the end of the timeframe in the amplitude data (Figure 10). This occurs where there was not sufficient contrast of the interface for the image processing algorithm to detect, e.g. Figure 9C. An exponential model of the form of Equation 2 was fit to the data where $\eta \ll \lambda$ (Figure 6, $R^2 = 0.998$). In this preliminary analysis, no satisfactory fit was found for data where

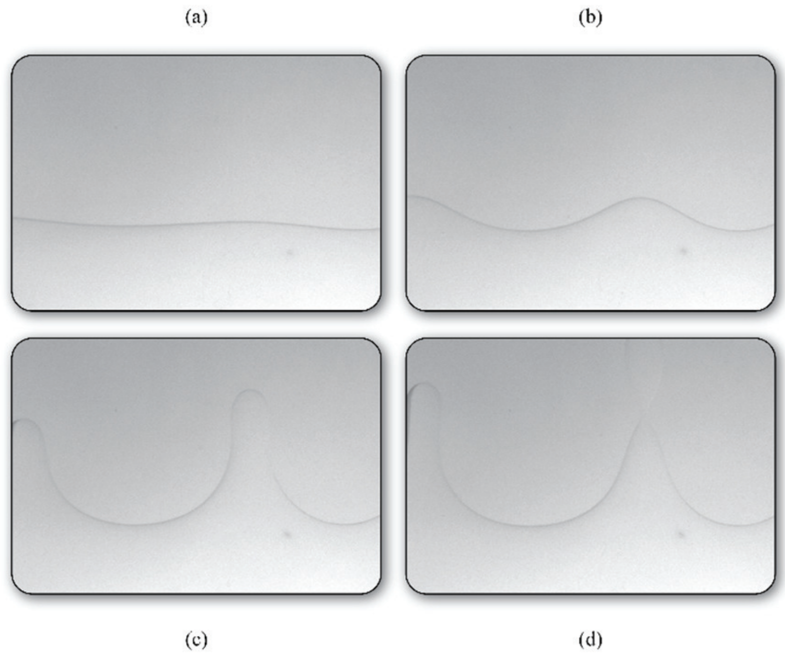

Fig. 9 Frames from video of the mixing experiment with six temperature probes. (a) 600 s – shows the beginning of a wave-like form, (b) 750 s – shows more amplitude growth, (c) 840 s – shows a spike right before necking begins to occur, (d) 853 s – shows necking of the right spike, with a bubble about to break off.

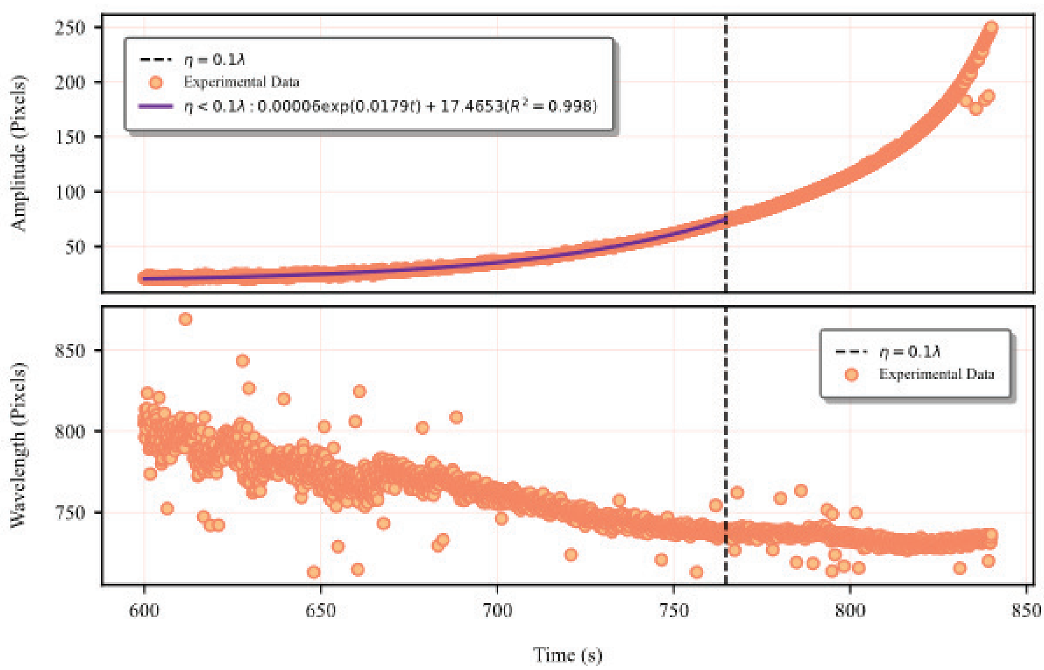

Fig. 10 The amplitude (top) and wavelength (bottom) determined from the mixing experiment video images. A dashed black line indicates the point in time where $\eta = 0.1\lambda$, which was the threshold used to distinguish the period when $\eta \ll \lambda$ and when $\eta \approx \lambda$. A model form from the literature (Equation 2) was fit the amplitude data where $\eta \ll \lambda$.

$\eta \approx \lambda$, but the growth is nonlinear, which disagrees with classical linear RTI growth reported in literature [7, 8]. The wavelength calculations showed a decrease during the initial period when $\eta \ll \lambda$, but approached steady-state as η continued to increase.

Discussion

Single-fluid calibration experiments were used to characterize of the microwave field and each fluid's temperature response to it. Given the large microwave penetration depths of both fluids compared to the fluid vessel size, Figure 5 suggests that it is possible that the microwave field was not uniform within the cavity and further investigation of this matter should be performed. The uneven microwave field could have been the generator of the initial perturbation at the fluid interface.

It was originally hypothesized that the temperature response of the fluids in the single-fluid experiment would be comparable to that of the mixing experiment; however, the Atwood number estimated from the single-fluid data never turned positive to indicate the system would become unstable. The soybean oil increased in temperature faster than PDMS, which is explained by soybean oil having a dielectric loss about 5 times greater than PDMS with a similar heat capacity and complex permittivity [14, 15, 16, 17, 18]. The dielectric loss quantifies the dissipation of electromagnetic energy through a fluid, heat capacity indicates the amount of energy required to change the temperature of the fluid, and the complex permittivity determines the reduction of the electromagnetic field intensity when it enters a material. In reference to Figure 1, this led to the soybean oil maintaining a lower density in comparison to the 7 cSt PDMS. In the future when selecting fluids for microwave VED-driven RTI, both the dielectric constant and the relationship between temperature and density need to be considered for identifying a fluid pair that will undergo density inversion with VED.

The temperature probe data from the mixing experiment indicated heat transfer from the soybean oil to the PDMS due to conduction at the fluid-fluid interface; this is supported by the soybean oil decreasing in temperature closer to the interface and the PDMS increasing in temperature closer to the interface. This supports the development of RTI captured by the video despite the simple estimation of the At remaining negative. Future work should identify fluids in which bulk density inversion, rather than localized density inversion, can be achieved.

Wave amplitude growth in the $\eta \ll \lambda$ region of the video appears consistent with the literature description of exponential growth (Equation (2)). In the $\eta \approx \lambda$ region, the At continued to change and deviation from the literature description of growth was observed; however, this stage of growth is not well understood [7]. Since there is conduction between fluids over the timescale of the reported experiment, further investigation is required to understand the late stage growth behavior and identify the assumptions used in traditional RTI models that are not valid and formulate an alternative growth model.

Conclusions

Advancements were made to improve an experiment involving microwave heating of two immiscible fluids intended to aide modeling efforts of VED-driven, variable At RTI for ICF applications. Temperature measurements were collected during heating to characterize the interactions between the microwave field and fluid system. It was found that the fluids heated a significantly different rates and conduction between the two fluids drove the instability; this was in opposition to the intended preferential heating and buoyancy-driven mixing caused by VED alone. Further work to select fluids that would exhibit the desired preferential heating and density subsequent density inversion is needed. An image processing workflow was developed to extract the wavelength and amplitude of the wave-like fluid interface over time. Preliminary analysis shows behavior consistent with the classical RTI literature when the amplitude was much less that the wavelength; however, classical linear RTI behavior was not observed when the amplitude and wavelength were similar orders of magnitude. Future work that remains before these experiments can be used to validate mixing models with VED source terms includes imposing initial conditions to the two-fluid interface, better characterizing the conduction and viscous effects present in experiment, and further extraction of relevant video and temperature data to better inform modeling. Experiments performed at different microwave power levels and investigation into the uniformity of the microwave field uniformity would also further elucidate the performance of the experimental setup for VED-driven RTI.

Acknowledgments The authors would like to thank RayVen Gonzales for collecting the density and viscosity measurements, Brandon Wilson for his advisement on experimental relevance to simulations, and Jason Martinez for his assistance with the experimental apparatus. This research was funded by Los Alamos National Laboratory (LANL) through the Engineering Institute's Los Alamos Dynamics Summer School. The Engineering Institute is a research and education collaboration between LANL and the University of California San Diego's Jacobs School of Engineering. This collaboration seeks to promote multidisciplinary engineering research that develops and integrates advanced predictive modeling, novel sensing systems, and new developments in information technology to address LANL mission relevant problems.

References

1. McGrail, P.B., T.H. Schaef, A.M. Ho, Y. Chien, J.J. Dooley, C.L. Davidson, Potential for carbon dioxide sequestration in flood basalts. Journal of Geophysical Research-Solid Earth, 2006. 111(B12).
2. Kennedy, A., S. Tadesse, J. Nunes, A. Reznik, Influence of microwave heating on liquid-liquid phase inversion and temperature rates for immiscible mixtures. Journal of Microwave Power and Electromagnetic Energy, 2011. 45(1): p. 5–14.
3. Joseph, D.D., J. Belanger, and G.S. Beavers, Breakup of a liquid drop suddenly exposed to a high-speed airstream. International Journal of Multiphase Flow, 1999. 25(6-7): p. 1263–1303.
4. Varga, C.M., J.C. Lasheras, and E.J. Hopfinger, Initial breakup of a small-diameter liquid jet by a high-speed gas stream. Journal of Fluid Mechanics, 2003. 497: p. 405–434.
5. Chen, H.B., B. Hilko, and E. Panarella, The Rayleigh-Taylor instability in the spherical pinch. Journal of Fusion Energy, 1994. 13(4): p. 275–280.
6. Lindl, J., Development of the indirect-drive approach to inertial confinement fusion and the target physics basis for ignition and gain. Physics of Plasmas, 1995. 2(11): p. 3933–4024.
7. Youngs, D. and A. Cook, Rayleigh-Taylor instability and mixing. Scholarpedia, 2009. 4(2).
8. Dimonte, G., Dependence of turbulent Rayleigh-Taylor instability on initial perturbations. Physical Review E, 2004. 69(5).
9. Joshi, A., M.C. Radhakrishna, and N. Rudraiah, Rayleigh-Taylor instability in dielectric fluids. Physics of Fluids, 2010. 22(6).
10. Wachtor, A.J., V. Mocko, D.J. Williams, M.P. Goertz, F.F. Jebrail, Buoyancy driven mixing of miscible fluids by volumetric energy deposition of microwaves. Journal of Microwave Power and Electromagnetic Energy, 2013. 47(3): p. 210–223.
11. Wachtor, A.J., V. Mocko, F.F. Jebrail, M.J. Andrews, On buoyancy driven mixing by volumetric microwave energy deposition. International Journal of Heat and Mass Transfer, 2015. 86: p. 443–454.
12. Root, P.R., Engen, K.R., Mejia, R., Wilson, B.M., and Wachtor, A.J., Volumetric energy deposition driven Rayleigh-Taylor instability experiments, in 9th Thermal and Fluids Engineering Conference. 2024: Partially Online and at Oregon State University, OR.
13. Roberts, C., A. Graham, M. Nemer, L. Phinney, R.M. Garcia, M. Soehnel, E.K. Stirrup, Physical properties of low-molecular weight polydimethylsiloxane fluids. 2017.
14. Zhou, X., Y. Gezahegn, S. Zhang, Z. Tang, P.S. Takhar, P.D. Pedrow, S.S. Sablani, J. Tang, Theoretical reasons for rapid heating of vegetable oils by microwaves. Current Research in Food Science, 2023. Volume 7.
15. Pen~aloza-Delgado, R., J.L. Olvera-Cervantes, M.E. Sosa-Morales, T.K. Kataria, A. Corona-Chavez, Dielectric characterization of vegetable oils during a heating cycle. Journal of Food Science and Technology, 2021. 58(4): p. 1480–1487
16. Du, P., X. Lin, and X. Zhang, *Dielectric constants of PDMS nanocomposites using conducting polymer nanowires,* in *16th International Solid-State Sensors, Actuators and Microsystems Conference.* 2011: Beijing, China.
17. Fasina & Z. Colley, *Viscosity and specific heat of vegetable oils as a function of temperature: 35°C to 180°C.* International Journal of Food Properties, 2008. **11**(4): p. 738–746
18. Wypych, G., *PDMS polydimethylsiloxane.* Handbook of Polymers, 2012. p. 328–332